Optics Letters

L-band mode-locked fiber laser using all polarization-maintaining nonlinear polarization rotation

Guanyu Ye,[1,2] Kin Kee Chow,[3] Bowen Liu,[1,2] Maolin Dai,[1,2] Yifan Ma,[1,2] Takuma Shirahata,[1,2] Shinji Yamashita,[2] and Sze Yun Set[1,*]

[1]Research Center for Advanced Science and Technology, The University of Tokyo, 4-6-1 Komaba, Meguro-Ku, Tokyo 153-8904, Japan
[2]Department of Electrical Engineering and Information Systems, The University of Tokyo, Bunkyo-Ku, Tokyo 113-8656, Japan
[3]Department of Engineering, Manchester Metropolitan University, John Dalton Building, Chester Street, Manchester M1 5GD, UK
*set@cntp.t.u-tokyo.ac.jp

Received 3 July 2023; revised 3 August 2023; accepted 15 August 2023; posted 16 August 2023; published 5 September 2023

For the first time, to the best of our knowledge, in the soliton regime, we demonstrate an L-band fiber laser mode-locked by all polarization-maintaining (all-PM) nonlinear polarization rotation (NPR). A numerical study suggests that lengthening the NPR section boosts modulation depth and lowers saturation power of the artificial saturable absorber (SA). With the longest NPR section to date (21 m), the laser emits 1.25-ps soliton pulses at 1584.2 nm and a 3.9-MHz repetition rate. Our laser provides a promising L-band seed source, exhibiting improved repeatability and stability compared with non-PM L-band pulse fiber lasers.

https://doi.org/10.1364/OL.498865

Ultrafast fiber lasers have gained tremendous research interest due to their strong potential in various fields, such as micromachining, metrology, and optical communications [1,2]. L-band (1565 nm to 1625 nm) mode-locked fiber lasers (MLFL) offer significant advantages in communications [3], spectroscopy [4], and equivalent-time optical sampling [5]. Equivalent-time sampling enables the acquisition of high-speed signals with a sampling rate significantly lower than the frequency of the signal itself, effectively making high-frequency measurements possible with slower sampling rates [6,7]. An L-band pulse laser also can provide 800 nm by second harmonic generation to replace the bulky Ti:Sapphire laser [8]. Over the past decade, there has been significant research on L-band MLFLs. A material saturable absorber (SA) including semiconductor saturable absorber mirror [9], carbon nanotube [10], graphene [11], and topological insulator [12] has been implemented for L-band mode-locking. An artificial SA such as nonlinear polarization rotation (NPR) [13], nonlinear loop mirror [14], and nonlinear multimode interference [15] has also been reported. However, in those studies, the non-polarization-maintaining (PM) configuration makes the laser susceptible to environmental perturbations, and the polarization controller (PC) in the laser cavity impairs the repeatability and reliability.

To address this issue, one alternative solution is to realize the NPR in all-PM fibers (all-PM NPR). Extensive research has been conducted on all-PM NPR mode-locking in the 1-μm wavelength range, including the regimes of all-normal dispersion (ANDi) and dispersion managed (DM). The high peak power of the pulses in the ANDi and DM regimes provides sufficient nonlinearity for NPR mode-locking. Nielsen and Keiding were the first to propose an all-PM NPR laser generating noise-like pulses in 2007 [16], while Szczepanek *et al.* achieved the first dissipative solitons in 2017 [17]. Reflection type all-PM NPR lasers incorporating Faraday rotation mirrors have also been reported [18,19].

However, achieving all-PM NPR mode-locking in the 1.5-μm spectrum regime is challenging, due to the limitations of the pulse peak power and Kerr nonlinearity. To address this, research has focused on increasing the pulse peak power. Optimizing the cavity dispersion in the DM regime is one possible solution [20]. Another method involves fabricating the NPR section using a PM erbium-doped fiber (EDF) to amplify the pulse and achieve the required peak power for NPR mode-locking [21]. In contrast, there has been limited research in the all-anomalous dispersion regime. Only one study by Z. Peng *et al.* has been reported [22], through employing a PM EDF in the NPR section. The laser exhibits sub-micro watt power at the C-band. As of now, there has been no report of a fiber laser mode-locked by all-PM NPR in the L-band. To expand the viability of all-PM NPR mode-locking in the all-anomalous dispersion regime, we present an MLFL delivering soliton pulses centered at 1584.2 nm. To the best of our knowledge, this is the first demonstration of an L-band pulse laser achieved using this approach.

Figure 1 shows the experimental setup of the all-PM NPR mode-locked fiber laser, comprising solely PM fibers and PM components. The laser cavity is composed of two main parts: the NPR section located on the right and the ring cavity positioned on the left. In the ring cavity parts, a slow-axis working PM tap isolating wavelength-division multiplexing (PM-TIWDM) functions as a polarizer, wavelength-division multiplexer, isolator, and output tap of 20%. The gain medium of 1.4-m PM-EDF (Nufern ESF-7/125) is backward pumped by a 980-nm laser

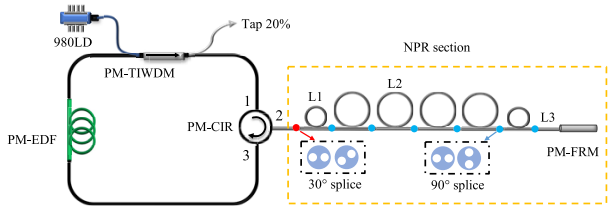

Fig. 1. Experimental setup of the all-PM NPR MLFL.

diode (LD) through the PM-TIWDM. The remaining passive fibers are the PANDA PM fiber (Fujikura SM15-PS-U25A). A slow-axis working PM circulator (PM-CIR) functions as a polarizer and isolator to ensure unidirectional propagation. The laser operates in the clockwise direction.

The NPR section in Fig. 1 consists of a 21-m polarization-maintaining fiber (PMF) and a PM Faraday rotation mirror (PM-FRM). Linear polarized light propagates from port 1 to port 2 through the PM-CIR along the slow-axis of the PMF. After a 30° angle splicing, the light splits into two orthogonally polarized components with unequal pulse energy. During their round trip through the 21-m PMF, two light components undergo different phase shifts due to the cross-phase modulation (XPM) and self-phase modulation (SPM), leading to a difference in polarization states between the pulse peak and wings. During propagation in the PMF, the two orthogonally polarized components exchange roles along the fast or slow axis in each segment, improving temporal overlap to enhance the XPM effect. The PM-CIR acts as a polarizer, inducing polarization-dependent nonlinear loss on both pulse peak and wings. Consequently, the NPR section functions as an artificial SA for mode-locking.

The 21-m PMF of the NPR section is divided into seven segments by six 90° angle splicing. The length of each segment from the 30° angle splicing point to the FRM (from left to right) is 2 m (L1), 4 m (L2), 4 m, 4 m, 4 m, 2 m, and 1 m (L3), respectively. The loss of each angle splicing is approximately 0.05 dB. The total cavity length is approximately 50 m, and the net dispersion is estimated to be -1.03 ps^2 at 1550 nm, indicating that the laser is operating in the soliton regime. In our reflection-configured NPR section, precisely controlling the fiber length is not required. The FRM rotates the polarization states of the two components by 90°, causing them to travel equal lengths along each axis of the PMF during a round trip. This naturally compensates for the walk-off induced by the PMF's birefringence [18].

The laser self-starts by directly ramping up the pump power. Initially at 260 mW, it operates in a multi-pulse regime, presenting 3 to 4 pulses on the oscilloscope. Reducing the pump to 95 mW transitions the laser to a stable mono-pulse operation, with an average output power of 120 μW. Amplified spontaneous emission (ASE) noise is observed on the spectrum. The optical spectrum in linear scale (μW) from 1500 nm to 1600 nm is shown in Fig. 2. The inset shows the spectrum in logarithmic scale (dBm). The ASE noise accounts for approximately 15% of the total output power. Therefore, the estimated average output power of the L-band soliton pulse is 102 μW. The observed ASE noise at 1530 nm is likely due to imperfections in components such as the PM-circulator and FRM. Additionally, the higher gain of the EDF at this wavelength compared with the L-band may also contribute to the ASE noise. Potential solutions include the incorporation of a longer EDF or the adjustment of the EDF's gain profile to lower the gain in the C-band.

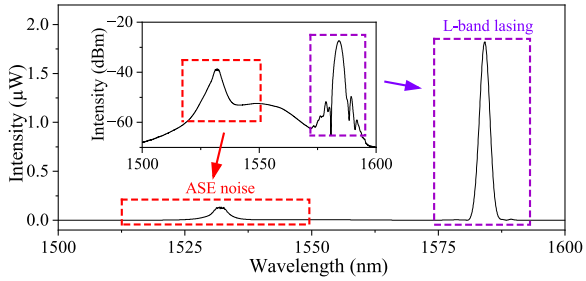

Fig. 2. Overall optical spectrum on linear and logarithmic (inset) scale.

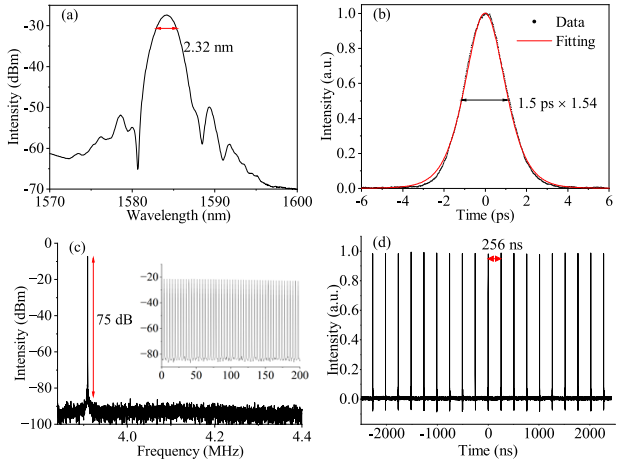

Fig. 3. Laser output characteristics: (a) optical spectrum; (b) AC trace (after 5-m PMF); (c) RF spectrum (RBW,100 Hz), inset shows harmonic RF spectrum (RBW, 10 kHz); (d) oscilloscope trace.

The output spectrum of the L-band soliton is depicted in Fig. 3(a), centering at 1584.2 nm with a full width at half maximum (FWHM) spectrum bandwidth of 2.32 nm. The autocorrelation (AC) trace was captured by directly recording the laser's original output with an autocorrelator (Femtochrome FR-103XL) and an oscilloscope (RIGOL MSO8104). The oscilloscope was configured in average mode with 128 times of averaging. To estimate the actual intra-cavity pulse width, we measured the AC after the output pulse propagating through different lengths of PMF: 5 m, 3 m, and 1 m. In Fig. 3(b), the AC raw data of the output after 5-m PMF exhibits an excellent fit to a squared hyperbolic secant (sech^2) shape, inferring a FWHM pulse width of 1.5 ps. The pulse width of the output pulse traversing 3 m and 1 m is estimated to be 1.4 ps and 1.3 ps, respectively, indicating a chromatic dispersion induced pulse broadening of 0.5 ps after 1 m of PMF propagation. Given the low peak power, only the chromatic dispersion is considered for the output pulse propagation in the PMFs. The PMF's GVD parameter of 23 ps/(nm·km) at 1.6 μm [23] and a FWHM bandwidth of 2.32 nm are considered. The FWHM width of the output is estimated to broaden to 0.053 ps for 1 m of PM propagation, which aligns well with the measurements and validates our approximation. Therefore, the intra-cavity pulse has an estimated FWHM of 1.25 ps and a time-bandwidth product of 0.346, indicating a nearly transform limited pulse.

The radio frequency (RF) spectrum is measured using a photodetector (New Focus 1611) and an electrical spectrum analyzer (RIGOL RSA3045). Figure 3(c) presents the RF spectrum with

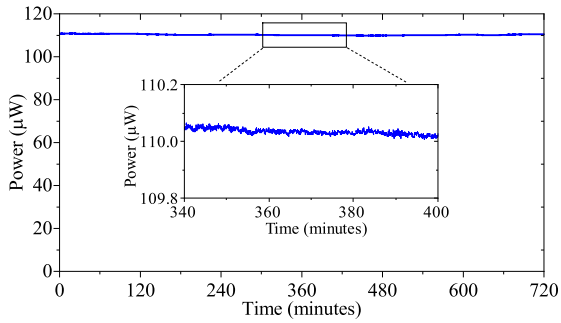

Fig. 4. Average output power of the laser for 12 hours.

a resolution bandwidth (RBW) of 100 Hz, exhibiting high pulse stability indicated by the 75-dB signal-to-noise ratio (SNR). The central frequency of 3.9 MHz aligns with an approximately 50-m cavity length. The inset depicts a harmonic RF spectrum with an RBW of 10 kHz, confirming the operation in a single-pulse regime. Figure 3(d) shows the oscilloscope trace, and the pulse period of 256 ns is in accordance with the fundamental repetition rate of 3.9 MHz. Given the output ratio of 20%, the intra-cavity power is estimated to be 0.5 mW, while the peak power is approximately 100 W. The challenges in achieving mode-locking by the all-PM NPR could be attributed to the relatively low peak power.

The laser consistently sustained L-band mode-locking over two days. During the 12-hour stability test, we operate the laser at a constant 225-mA current (approximately 95-mW pump power), without any special temperature or vibration control (Fig. 4). The average output power has been measured by a light wave multimeter (Agilent 8163A) and optical head (Hp 81524A). A short-term stability assessment over 2 minutes shows an average power of 110.05 μW and a root mean square (rms) stability of 0.005%. These results demonstrate the exceptional short-term stability of the laser and robustness against environmental perturbations. The rms stability over 12 hours is approximately 0.27%. The slight power drift could be attributed to C-band ASE noise, and the temperature variation between daytime and nighttime. This laser's sensitivity to temperature changes, potentially due to non-optimized cavity parameters such as tap ratio, cavity length, and losses. Temperature changes cause variations in the cavity length, acting as additional wave plates to influence the NPR effect [17]. This may contribute to the laser self-starting by external intervention.

The low output power is attributed to the low-gain of the EDF at the L-band. As the NPR section solely consists of passive PM fiber, increasing the output power could be achieved by using an L-band EDF, such as the Nufern EDFL 980/1480 series, or optimizing the gain profile by combining different EDFs [24]. In our laser, we employ a standard PM-EDF and use the gain curve shift property by a longer EDF length and low pump power [25,26].

A numerical study is conducted to investigate the transmission properties of the NPR section. The simulation diagram is shown in Fig. 5(a). A sech^2 pulse with an FWHM of 1.2 ps, and a varying peak power ranging from 1 W to 2 kW is used as the input. The pulse propagation in the PMF is modeled by the coupled-mode nonlinear Schrödinger equations [23] and solved via split-step Fourier method. The total transmission of the pulse energy at varying peak power levels is obtained. The total PMF length is depicted as 21 m in Fig. 5(a), but this value varies from 2 to 22 m in the simulation, while maintaining a 7-segment structure and

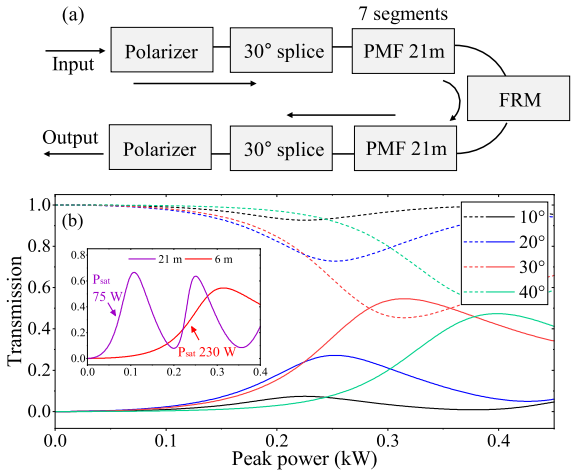

Fig. 5. (a) Schematic diagram for simulation, (b) transmission for four spliced angles (6-m NPR length) along slow (solid) and fast (dashed) axes. Inset shows slow-axis transmission with 30° splicing, 21-m (purple) and 6-m (red) NPR length.

the same length ratio. The simulation focuses on the modulation depth (MD) and saturation power (P_{sat}), which is based on the transmission property of the all-PM NPR section [18].

Figure 5(b) shows the transmission curve of the NPR section with 6-m PMF, a typical length used in prior studies, for four different spliced angles. The solid and dashed lines denote transmission along the PMF's slow and fast axes, respectively. The solid lines show SA property until the peak power reaches a limit, at which point a transition to reverse SA property is observed. In contrast, the dashed line behaves in an opposite manner. As the PM-CIR operates only on the slow-axis, the solid line represents the transmission of the NPR section in the experiment. Our primary focus is on the SA property. Optimizing a saturable absorber's MD and P_{sat} is crucial for mode-locking. Saturable absorbers with a small MD and high P_{sat} may cause continuous wave lasing, while low P_{sat} may lead to pulse-splitting. Adjusting the spliced angle can efficiently control these parameters. The NPR section with 30° spliced angle (red line) exhibits the highest MD and a relatively higher P_{sat}, while the 10° (black line) exhibits the lowest P_{sat} and lowest MD. There is a trade-off between the two parameters, and it is difficult to find a spliced angle that simultaneously yields a large MD and a small P_{sat}.

To overcome the challenge, we have developed an alternative approach to tune the SA property by optimizing the NPR section length. The inset in Fig. 5(b) shows the transmission of the NPR sections with 30° splicing and lengths of 21 m (purple line) and 6 m (red line). The P_{sat} decreases by approximately three times, from 230 to 75 W. The MD and P_{sat} versus NPR section length is illustrated in Fig. 6, with a fixed 30° splicing. MD increases and P_{sat} consistently decreases with increasing length. The P_{sat} significantly reduces below 5 m and stabilizes beyond 20 m, suggesting a limit of reduction via length increase. Given the potentially insufficient pulse peak power, lowering P_{sat} of an SA emerges as a feasible strategy for achieving mode-locking for L-band solitons with low peak power.

Our proposed approach involves a longer NPR section length to lower the P_{sat} and slight tuning of MD and P_{sat} through adjustment of the spliced angle. Additionally, a longer total cavity length reduces the repetition rate, subsequently enhancing the intra-cavity pulse energy and peak power, contributing to

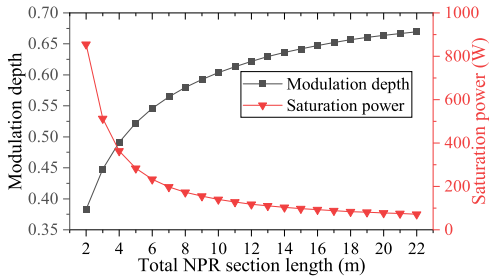

Fig. 6. Simulation results: MD and P_{sat} versus total NPR section length.

NPR mode-locking. In the simulation, the estimated P_{sat} for a 21-m NPR section length is 75 W, close to the experimental value of 100 W observed. The steep slope of the transmission curve near the P_{sat} also facilitates the all-PM NPR mode-locking [27]. We have also tested NPR section lengths of 4 m, 6 m, and 10 m. Despite adjusting the splice angle, mode-locking is not accomplished. This could be attributed to the elevated P_{sat} and diminished pulse peak power associated with a short NPR section, both of which impede the NPR mode-locking.

In summary, we have presented the first all-PM NPR fiber laser, delivering soliton pulses at 1584.2 nm in the L-band. Comprising solely a passive fiber and at a record length of 21 m, our NPR section enables a laser with an FWHM bandwidth of 2.32 nm and an RF SNR of 75 dB. Our study reveals that an extended NPR section can lower the saturation power and augment the modulation depth, thus promoting robust mode-locking. Our all-PM laser potentially provides an L-band seed source for applications such as equivalent-time optical sampling.

Funding. Japan Society for the Promotion of Science (18H05238, 22H00209, 23H00174); Core Research for Evolutional Science and Technology (JPMJCR1872).

Acknowledgments. Sze Yun Set thanks Mr. Hideru Sato and Mr. Raymond Chen for their kind personal donation for this research work. Kin Kee Chow was partially supported by the Daiwa Anglo-Japanese Foundation grant (11592/13817).

Disclosures. The authors declare no conflicts of interest.

Data availability. Data underlying the results presented in this paper are not publicly available at this time but may be obtained from the authors upon reasonable request.

REFERENCES

1. J. Limpert, F. Roser, T. Schreiber, and A. Tunnermann, IEEE J. Select. Topics Quantum Electron. **12**, 233 (2006).
2. M. E. Fermann and I. Hartl, IEEE J. Select. Topics Quantum Electron. **15**, 191 (2009).
3. G. Rademacher, R. S. Luís, B. J. Puttnam, R. Ryf, S. van der Heide, T. A. Eriksson, N. K. Fontaine, H. Chen, R.-J. Essiambre, and Y. Awaji, in *Optical Fiber Communication Conference* (Optica Publishing Group, 2020), paper Th4C. 5.
4. J. Kang, X. Wei, S. Tan, A. H. Tang, K. K. Tsia, and K. K. Wong, in *CLEO: Science and Innovations* (Optica Publishing Group, 2016), paper SM4P. 2.
5. S. Lefrancois, Y. Paquot, B. J. Eggleton, H. C. Nguyen, D. Wang, S. Y. Set, D.-Y. Choi, B. Luther-Davies, and S. J. Madden, in *Asia Communications and Photonics Conference* (Optica Publishing Group, 2014), paper AF4A. 3.
6. J. Li, J. Hansryd, P. O. Hedekvist, P. A. Andrekson, and S. N. Knudsen, in *Optical Fiber Communication Conference and Exhibit*, Technical Digest Postconference Edition (IEEE Cat. 01CH37171) (IEEE, 2001), paper PD31-PD31.
7. M. Westlund, H. Sunnerud, M. Karlsson, and P. A. Andrekson, J. Lightwave Technol. **23**, 1088 (2005).
8. M. Hofer, M. Fermann, A. Galvanauskas, D. Harter, and R. S. Windeler, Opt. Lett. **23**, 1840 (1998).
9. H. Zhang, D. Tang, X. Wu, and L. Zhao, Opt. Express **17**, 12692 (2009).
10. Z. Sun, A. Rozhin, F. Wang, V. Scardaci, W. Milne, I. White, F. Hennrich, and A. Ferrari, Appl. Phys. Lett. **93**, 061114 (2008).
11. Y. Meng, A. Niang, K. Guesmi, M. Salhi, and F. Sanchez, Opt. Express **22**, 29921 (2014).
12. Y. Meng, G. Semaan, M. Salhi, A. Niang, K. Guesmi, Z.-c. Luo, and F. Sanchez, Opt. Express **23**, 23053 (2015).
13. J. L. Luo, L. Li, Y. Q. Ge, X. X. Jin, D. Y. Tang, S. M. Zhang, and L. M. Zhao, IEEE Photonics Technol. Lett. **26**, 2438 (2014).
14. K. Guesmi, Y. Meng, A. Niang, P. Mouchel, M. Salhi, F. Bahloul, R. Attia, and F. Sanchez, Opt. Lett. **39**, 6383 (2014).
15. L. Li, Z. Wang, D. Wang, and F. Yang, IEEE Photonics Technol. Lett. **31**, 647 (2019).
16. C. K. Nielsen and S. R. Keiding, Opt. Lett. **32**, 1474 (2007).
17. J. Szczepanek, T. M. Kardaś, C. Radzewicz, and Y. Stepanenko, Opt. Lett. **42**, 575 (2017).
18. J. Szczepanek, T. M. Kardaś, C. Radzewicz, and Y. Stepanenko, Opt. Express **26**, 13590 (2018).
19. M. Yu, Z. Cheng, C. Hong, Y. Shi, Z. Peng, M. Wang, and P. Wang, Opt. Express **28**, 32764 (2020).
20. X. Liu, Q. Li, D. Pan, F. Ye, B. A. Malomed, and H. Fu, J. Lightwave Technol. **39**, 7509 (2021).
21. L. Zhou, Y. Liu, G. Xie, W. Zhang, Z. Zhu, C. Ouyang, C. Gu, and W. Li, Appl. Phys. Express **12**, 052017 (2019).
22. Z. Peng, Z. Cheng, X. Bu, C. Hong, H. Li, Y. Shi, and P. Wang, IEEE Photonics Technol. Lett. **30**, 2111 (2018).
23. G. P. Agrawal, *Nonlinear Fiber Optics*, 5th ed. (Elsevier/Academic, 2013).
24. Z. Wang, L. Zhan, X. Fang, C. Gao, and K. Qian, J. Lightwave Technol. **34**, 4128 (2016).
25. S.-F. Lin and G.-R. Lin, Opt. Express **22**, 22121 (2014).
26. J. Jiang, Y. Ma, M. Wang, Q. Huang, L. Dai, Z. Huang, Y. Liu, and C. Mou, Results Opt. **10**, 100360 (2023).
27. W. Hänsel, H. Hoogland, M. Giunta, S. Schmid, T. Steinmetz, R. Doubek, P. Mayer, S. Dobner, C. Cleff, M. Fischer, and R. Holzwarth, Appl. Phys. B **123**, 41 (2017).